Connecting the phase-field-crystal model of electromigration with electronic and continuum theories

Nan Wang [1,2,3,*] Hong Guo,[2] and Nikolas Provatas[2]

[1]*Department of Materials Science and Engineering, Guangdong Technion–Israel Institute of Technology, Shantou 515063, China*

[2]*Department of Physics, McGill University, Montreal, Québec H3A 2T8, Canada*

[3]*Department of Materials Science and Engineering, Technion–Israel Institute of Technology, Haifa 32000, Israel*

(Received 3 June 2019; revised 6 October 2021; accepted 3 November 2021; published 17 November 2021)

Electromigration (EM) is the motion of lattice atoms under high-density electric current. It is an important mechanism for structural changes in nanoelectronic devices and a major contributor to the electroplastic effect in structural metals. Recently, a phase-field-crystal (PFC) model for studying EM in metals was developed and shown to successfully capture many important EM-driven structural evolutions at experimentally relevant timescales. In this work, connections between the previous PFC EM model and existing EM theories are established. It is shown that the PFC model can be linked to both the electron-density-based quantum EM theory and the drift-diffusion-based continuum EM theory, therefore filling an important gap in the theoretical and computational study of EM-related phenomena. The numerical method for implementing the PFC EM model is discussed in detail. The well-established Blech effect is quantitatively reproduced using the model.

DOI: 10.1103/PhysRevMaterials.5.115002

I. INTRODUCTION

Electromigration (EM) is a process of both theoretical and technological importance [1–5]. On the technology side, the EM process has been known as a leading failure mechanism of integrated electric circuits and a major contributing factor in electroplasticity, and recently it has been used to produce metallic nanocontacts [6]. On the theory side, EM has been actively studied using quantum mechanical theories and continuum theories. Quantum mechanical studies have focused on the nature of EM force from scattering of conduction electrons [7–9], while the continuum works have mainly focused on predicting failure of current-carrying metal materials as the result of EM-driven atom migration over operation timescales [10–14].

As the dimensions of integrated circuits quickly approaches the nm scale, microstructural defects such as grain boundaries and surface steps become increasingly important in the EM process [6,15]. In the case of metallic nanocontacts, better control of the EM-driven thinning process is also critical [16]. Methods based on electronic density functional theory have been successfully used to study some microstructural effects on the EM process at nanoscales [9,17,18]. However, such methods are limited to small systems and cannot be used to study EM-driven microstructural dynamics in time, which are critical to both interconnect failure and electroplasticity. Therefore an efficient computational method that can track EM-driven microstructural change in nanoscale metals over diffusion timescale is highly desirable.

Recently, a phase-field-crystal (PFC) model motivated by classical density functional theory (CDFT) [19,20] was developed to study some well-established EM phenomena such as the Blech effect and void formation at a microstructural triple junction [21]. It offers a promising approach for tracking microstructural change in interconnects at atomic resolution over diffusion timescales. However, the EM driving force in this method is incorporated phenomenologically through an auxiliary field, which is proportional to local electric potential. While such a field is motivated by the fact that the EM force $f_{EM} = Z^* eE$, where Z^* is the effective EM charge and the electric field E is the gradient of electric potential, it does not provide at least a qualitative linkage toward electronic EM theories. Also, at the electron level, the EM wind force is a manifestation of electron-ion interactions that arise due to electron density response to an applied electric field [9,22]. The total EM force is a combination of the wind force and a direct force which comes from the interaction of ions with applied field. It is not entirely clear how the EM force, which is generated from ion-related interactions, could be incorporated in a PFC-type model where the basic ingredient is a density field describing neutral atoms rather than ions. At the continuum level, although the previous PFC EM model is shown to generate a stress response to EM-induced atomic currents which is qualitatively similar to the Blech effect, it is also not clear how the previous model can be quantitatively linked to the well-established drift-diffusion-based continuum EM theory.

In this paper, a connection between the previous PFC EM model and electronic EM theories is explained. It is shown that the PFC EM model can be derived from a CDFT-type theory previously used for liquid metal systems where both ion and electron densities are considered. The electron density is separated into a zero-field part and a field-induced deviation part; the first part is incorporated in the PFC model through the effective inter-ion interaction, and the field-induced deviation part, which is associated with the EM force due to electron-ion interactions, is incorporated using an effective

*Corresponding author: nan.wang@gtiit.edu.cn

EM potential which can be linked to the effective EM charge. One can thus recover the previous neutral-atom-based PFC EM model that incorporates an effective EM force. A connection to the continuum theory of EM-induced stress evolution is also discussed. It is shown that the PFC EM model has both the EM-driven and stress-driven atomic fluxes at the coarse-grained level, therefore quantitatively reproducing the Blech effect.

The remainder of this paper is organized as follows. The previous PFC EM model is briefly reviewed in Sec. II. The model is reinterpreted in order to connect it to quantum mechanical EM theories in Sec. III. The continuum EM theory and its relation to the newly interpreted PFC EM model is discussed in Sec. IV. Section V discusses the numerical algorithm used to solve the PFC EM model proposed in this work. Numerical results are demonstrated in Sec. VI together with our discussion. The last, summary section concludes this work.

II. PFC EM MODEL

Standard PFC methods begin as an approximation to the dynamical density functional theory (DDFT) [23]. Since both the ideal and the excess parts of the free energy in CDFT are expanded in the PFC model, the sharp particle density profile seen in CDFT is smoothed in the PFC method which greatly improves numerical efficiency in dynamical simulations. While maintaining some of the microscopic granularity of the CDFT, PFC methods can reach longer timescales and therefore have been used to study microstructure evolution [24,25], diffusional interface instabilities [26,27], and other time evolution problems in materials science that involve the interactions of defects on long time and length scales [28,29].

The previous PFC EM model starts with the following CDFT-type free energy functional,

$$\begin{aligned}\mathcal{F} = \frac{\Delta F}{k_B T\bar{\rho}} &= \int d\mathbf{R}\left[\frac{n(\mathbf{R})^2}{2} - \frac{n(\mathbf{R})^3}{6} + \frac{n(\mathbf{R})^4}{12}\right] \\ &- \frac{1}{2}\int n(\mathbf{R}_1)\left[\int C^{(2)}(\mathbf{R}_1-\mathbf{R}_2)\, n(\mathbf{R}_2) d\mathbf{R}_2\right] d\mathbf{R}_1 \\ &+ \sum_{m=3}^{4}\frac{1}{m}\left[\int d\mathbf{R}_1 \ldots d\mathbf{R}_m \chi^{(m)}(\mathbf{R}_1,\ldots,\mathbf{R}_m)\right. \\ &\left.\times n(\mathbf{R}_1)\ldots n(\mathbf{R}_m)\right] + \int n(\mathbf{R}) U_{\text{eff}}(\mathbf{R}) d\mathbf{R}, \end{aligned} \tag{1}$$

where the density parameter $n(\mathbf{R}) = (\rho - \bar{\rho})/\bar{\rho}$, where $\bar{\rho}$ is a reference density. The first line is a Taylor expansion of the CDFT ideal part free energy density, while in the second line, the pair correlation function is simplified to $C^{(2)}(\mathbf{R}_1 - \mathbf{R}_2) = \delta(\mathbf{R}_1 - \mathbf{R}_2)\{1 - r - B_x(1 - \nabla^2_{\mathbf{R}_2})^2\}$. To capture the formation of voids in structural evolution, the third line follows Ref. [27] and includes higher-order multipoint correlations given by $\chi^{(3)} = (\alpha r + b)\chi(\mathbf{R}_1 - \mathbf{R}_2)\chi(\mathbf{R}_1 - \mathbf{R}_3)$ and $\chi^{(4)} = c\chi(\mathbf{R}_1 - \mathbf{R}_2)\chi(\mathbf{R}_1 - \mathbf{R}_3)\chi(\mathbf{R}_1 - \mathbf{R}_4)$, with $\chi(k) = \exp[-k^2/(2\lambda)]$ in reciprocal space. In the above expressions, B_x is proportional to the solid compressibility, λ is a constant that can be tuned to capture the thermodynamics of the material system, and r plays the role of an effective temperature, i.e., $r = f(T)$ [30]. The effective EM potential is written as $U_{\text{eff}}(\mathbf{R}) = A_{em}V(\mathbf{R})$, where $V(\mathbf{R})$ is electric potential. The coefficient is $A_{\text{em}} = n_{mf}Z^*e/(k_B T\bar{\rho}\Omega)$ with $n_{mf} = \int \chi(\mathbf{R} - \mathbf{R}')n(\mathbf{R}')d\mathbf{R}'$. The gradient of $V(\mathbf{R})$ gives local electric field E.

Microstructure evolution is described by the PFC density field $n(\mathbf{R})$ and follows the conserved dissipative dynamics given by

$$\frac{\partial n}{\partial t} = \nabla\cdot\left(\Gamma\nabla\frac{\delta\mathcal{F}}{\delta n}\right) + \eta, \tag{2}$$

where Γ is a mobility parameter, η a stochastic noise term satisfying the fluctuation-dissipation theorem $\langle\eta(\mathbf{R},t),\eta(\mathbf{R}',t')\rangle = -2(\Gamma/\bar{\rho}_i a^d)\nabla^2\delta(\mathbf{R}-\mathbf{R}')\delta(t-t')$ with a being the lattice constant of the crystal phase minimized by the PFC theory. Explicit temperature dependence in the noise has been scaled out [27]. Since the microstructure change is a rather slow process, the electric potential $V(\mathbf{R})$ is assumed to satisfy the flux conservation condition

$$\nabla\cdot(\sigma\nabla V) = 0, \tag{3}$$

where the conductivity $\sigma = \sigma_0$ in bulk metal and interpolates to other values in regions of other microstructure defects such as voids, grain boundaries, and dislocations.

III. CONNECTION TO QUANTUM MECHANICAL EM THEORIES

A. Density functional theories

Electronic density functional theory (DFT) is a widely used computational method for investigating electronic structures of quantum many-body systems in physics, chemistry, and materials science. In the field of electromigration, electronic DFT has been used to calculate the EM force and the effective EM charge in many materials.

In the electronic DFT, the total energy of an electronic system is [31]

$$E(\rho_e) = \int v(\mathbf{r})\rho_e(\mathbf{r})d\mathbf{r} + E_e(\rho_e), \tag{4}$$

where $v(r)$ is an external potential, ρ_e is electron density, and E_e is the total energy from electrons, which includes electron kinetic energy, exchange correlation energy, and direct Coulombic interactions. Without an external electric field, minimization of E gives a "textbook" solution of the electron density $\rho_e^0(r)$. The combination of the electron-ion interaction and the ion-ion Coulombic interaction is what gives an effective interatomic potential in metals [32,33].

In the CDFT, the free energy of an interacting system of atoms is [19,33]

$$F(\rho_a) = F^{\text{id}} + F^{\text{ex}} + F^{\text{ext}}, \tag{5}$$

where ρ_a is atomic density, F^{id} is the ideal free energy of noninteracting atoms, F^{ex} is the excess free energy, which includes atomic interactions, and F^{ext} is the contribution from the interaction between ρ_a and an external field. Using classical atoms, this CDFT formulation has been very successful in studies of liquids and solid-liquid phase transitions. In particular, it is capable of giving rise to a solid phase described

by an atomic density field that forms periodic lattices below a freezing temperature [34].

The two density functional formulations above have been previously combined to form a theory of liquid metals using metal ion and electron densities [33]. While the ions in that theory are similar to the atoms in the CDFT (and those used in molecular dynamics simulations), ionic interactions comprise a combination of Coulombic interactions between like ions and those between ions and electrons. Due to the timescale separation of electronic and ionic dynamics (Born-Oppenheimer approximation), ion interactions can be simplified by expressing them as the sum of the inter-ionic Coulombic potential and an additional potential contribution from a "frozen" electron distribution around the ions.

B. Electromigration force

In the presence of an external electric field, electromigration of metal ions is driven by two forces, an electron wind force which comes from scattering of conduction electrons from ion cores, and a direct force which is the Coulombic interaction between ions and the external field. In this part we mainly focus on the wind force, noting that the direct force due to screening effects is still being debated in the literature [6,35]. Also, instead of solving for the electron density under an external field and the associated wind force (which has been done in many previous studies), this section discusses how to effectively incorporates the EM force in a CDFT-type microstructure evolution model.

In an electron-ion binary system, the electron-ion interaction energy is $\int d\mathbf{R}\rho_i(\mathbf{R})\int V_{ie}(\mathbf{r}-\mathbf{R})\rho_e(\mathbf{r})d\mathbf{r}$ [33], where ρ_i is the ion density, ρ_e is the conduction electron density, V_{ie} is the interaction potential, $\mathbf{r}$ is the electron coordinate, and $\mathbf{R}$ is the ion coordinate. Under an external electric field, this interaction energy can be separated into two parts,

$$\begin{aligned}&\int \rho_i(\mathbf{R})\int V_{ie}(\mathbf{r}-\mathbf{R})\rho_e(\mathbf{r})d\mathbf{r}d\mathbf{R}\\&=\int \rho_i(\mathbf{R})\int V^*_{ie}(\mathbf{r}-\mathbf{R})\rho^0_e(\mathbf{r})d\mathbf{r}d\mathbf{R}\\&\quad+\int \rho_i(\mathbf{R})\int V^*_{ie}(\mathbf{r}-\mathbf{R})\rho^1_e(\mathbf{r})d\mathbf{r}d\mathbf{R},\end{aligned}\tag{6}$$

where ρ^0_e is the zero-field electron density (i.e., the electron density without external electric field), ρ^1_e is a small deviation of electron density from ρ^0_e induced by the external field, and the pseudopotential of the ion core V^*_{ie} is used on the right-hand side [22,33]. The first integral on the right is the standard electron contribution to the effective inter-ion potential [33], while the second integral on the right is an additional electron-ion interaction energy due to the external field. The wind force exerted on ions due to this additional energy is

$$\frac{\partial}{\partial\mathbf{R}}\int V^*_{ie}(\mathbf{r}-\mathbf{R})\rho^1_e(\mathbf{r})d\mathbf{r}=\int \rho^1_e(\mathbf{r})\frac{\partial V^*_{ie}(\mathbf{r}-\mathbf{R})}{\partial\mathbf{R}}d\mathbf{r},\tag{7}$$

which is the standard expression for wind force from the Hellmann-Feynman theorem [35]. Since electrons are "frozen" on the timescale of ion dynamics, one can integrate out the electron degrees of freedom $\int V^*_{ie}(\mathbf{r}-\mathbf{R})\rho^1_e(\mathbf{r})d\mathbf{r}=U(\mathbf{R})$, just as is done in the construction of effective inter-ion potential without external field. This result indicates that the effect of the wind force on ions can be written as a simple potential $U(\mathbf{R})$ that comes from the interaction between the ion core potential and the electron density *deviation* induced by the external electric field. This simple argument above is based on considering a bulk crystal, but it has been shown that the wind force on ions can also be seen as an external potential in the presence of vacancies [22] and microstructure defects (such as surface steps [35]). In the energy functional, this wind-force-induced energy can be simply written as $\int \rho_i(\mathbf{R})U(\mathbf{R})d\mathbf{R}$.

In general, the wind force on ions is a conservative force which can be seen as the gradient of a potential field [36] and can be calculated using well-established electronic methods [37].

The free energy functional for an ion system under an external potential is

$$\begin{aligned}\Delta F=k_BT\bar{\rho}_i\Bigg(&\int\{[1+n(\mathbf{R})]\ln[1+n(\mathbf{R})]-n(\mathbf{R})\}d\mathbf{R}\\&-\sum_{m=2}^{M}\frac{1}{m!}\int\prod_{j=1}^{m}n(\mathbf{R}_j)C_m(\mathbf{R}_1,\mathbf{R}_2,\ldots,\mathbf{R}_m)d\mathbf{R}_j\\&+\int n(\mathbf{R})U_{\rm eff}(\mathbf{R})d\mathbf{R}\Bigg),\end{aligned}\tag{8}$$

where k_BT is the thermal energy, $\bar{\rho}_i$ is a reference ion fluid density, $n(\mathbf{R})=(\rho_i-\bar{\rho}_i)/\bar{\rho}_i$, $C_m(\mathbf{R}_1,\mathbf{R}_2,\ldots,\mathbf{R}_m)$ is the m-point direct correlation function, and $U_{\rm eff}(\mathbf{R})$ is the external field. It is noted that ΔF has been tacitly scaled here by $\bar{\rho}_i$. On the right-hand side, the first integral is the ideal contribution, the second integral is the excess part, and the third integral is the contribution from the external field. Also, a constant contribution to the free energy from the reference density has been subtracted.

The EM direct force can be easily included in the external field term since it is a Coulombic interaction term. The wind-force-induced energy in the previous section can also be included in this external field term since it has the same form of $\int \rho_i(\mathbf{R})U(\mathbf{R})d\mathbf{R}$. To find the correct $U_{\rm eff}(\mathbf{R})$ that incorporates both the wind and the direct force, the easiest approach is to turn to the well-established effective-charge-based EM description where the EM force is averaged over the ion migration path [37]. In this way, one can simply approximate the $U_{\rm eff}$ by a linear function along the electron current direction such that the gradient of this function recovers the effective-charge-based EM force. Details about how to obtain the effective EM charge from quantum mechanical calculations can be found in Ref. [37].

Dissipative dynamics applied to Eq. (8) can be used to study the dynamical evolution of the density field in the presence of the effective EM potential [38]. However, this type of dynamical density functional theory (DDFT) calculation is computationally very expensive for calculations in the mesoscale time regime which is relevant to microstructure evolution in EM processes. The PFC model is therefore needed as a computationally efficient approximation.

Comparing the CDFT-based formulation above with the PFC EM model in the previous section, one can already clarify some key issues in the PFC model. First, the density

parameter in the PFC model is actually to be interpreted as the ion density, although it can still be well approximated as an atomic density. Second, the EM energy term in the PFC model is the product of the local ion density and a linear function proportional to local electric potential as described in the CDFT model in Eq. (8). It incorporates both the wind force from the electron-ion interaction and the direct force from the Coulombic interaction between the ion charge and the applied electric field through the effective EM charge.

IV. CONTINUUM EM THEORY

As demonstrated in the previous section, the PFC EM model is an approximation to the CDFT formulation based ion and electron densities. Its connection to the continuum EM theory is discussed in this section.

The continuum EM theory is formulated based on drift diffusion of lattice atoms under the EM force. EM-induced atomic flux is $J_{\rm em} = McZ^*eE$, where Z^*eE is the effective EM force, M is atomic mobility, and c is atom concentration (here the solid is seen as a mixture of atoms and vacancies). This atomic flux slowly transports lattice atoms from the upstream of the electron current to the downstream, and therefore induces atom pileup at the downstream and atom depletion at the upstream. When the conducting material is confined by other surrounding materials, the atom pileup or depletion produced by the EM-induced atomic current cannot be accommodated by volume expansion or shrinkage; hydrostatic pressure will develop in the conductor to locally accommodate additional atoms or vacancies through lattice deformation. This pressure, on the other hand, will also drive atomic motion by producing an atomic current from highly stressed regions to less stressed regions. The pressure-induced atomic current is expressed in 1 dimension (1D) as $J_p = -Mc\Omega dP/dx$, where Ω is atomic volume, x is the spatial coordinate along the current direction, and dP/dx is the gradient of the hydrostatic pressure P. The EM-induced atomic transport can be completely shut down if the pressure gradient satisfies $dP/dx = Z^*eE/\Omega$, which is known as the Blech effect.

The comparison of the PFC EM model introduced in previous sections with the straightforward current-balancing criterion in the continuum theory above is rather obscure. The rest of this section is therefore dedicated to establishing a connection between the PFC EM model and the continuum current-balance formulation.

One major difference between the PFC model and the continuum theory is the field variable used to describe the system evolution. While the continuum approach tracks the evolution of the atom concentration c, the PFC method works with the density parameter n. Another difference of the two approaches is the fundamental length scales in the description. Atomic spacing enters the PFC model through the two-point correlation function, but it is nowhere to be seen in the continuum drift-diffusion theory. These two differences also cannot be completely separated since the concentration in the continuum theory typically covers a spatial region which encompasses at least several atomic spacings.

Since the key feature in the continuum theory is the balance of the pressure-driven and the EM-driven atomic fluxes, one may start to build up the connection between the two methods by identifying these two fluxes in the PFC EM model.

Using the standard *one-mode approximation* of the PFC density field in a 2-dimensional (2D) solid phase [25], given by

$$n = A_1\left[\cos\left(\frac{2\pi x}{a}\right)\cos\left(\frac{2\pi y}{a\sqrt{3}}\right) - \frac{1}{2}\cos\left(\frac{4\pi y}{a\sqrt{3}}\right)\right] + n_0, \tag{9}$$

where $A_1 = \frac{2}{5}(-1 + 2n_0 - \sqrt{1 - 20r + 16n_0 - 16n_0^2})$, $a = 4\pi/\sqrt{3}$, and the average density is n_0, the unit-cell-averaged solid-state free energy density becomes

$$f_a = \frac{1}{V_0}\int_{V_0} F(n)dv, \tag{10}$$

where V_0 is the unit cell area, and $F(n)$ is the PFC free energy functional in Eq. (1) without the last EM term.

The chemical potential from the unit-cell-averaged PFC free energy is then $\mu_a^{PFC} = \frac{\partial f_a}{\partial n_0}$. Since n_{mf} in the PFC model is a long-range average of n, one can assume it is a constant over a unit cell and only varies significantly over a length scale much larger than the lattice spacing; one may also calculate the chemical potential using n_{mf},

$$\mu_{mf}^{PFC} = \frac{\partial f_a}{\partial n_{mf}}. \tag{11}$$

Since the model is formulated using the Helmholtz free energy and the solid phase is in equilibrium with the vapor phase during the EM process, the change of the solid phase Helmholtz free energy should be $dF = -PdV + \mu dN = 0$. The hydrostatic pressure in the system is then $P = \mu/\Omega$ since $dV = \Omega dN$. Local pressure in the PFC model can thus be expressed as

$$P = k_BT\bar{\rho}\mu_{mf}^{PFC}, \tag{12}$$

where $k_BT\bar{\rho}$ is the scaling factor from Eq. (1), and the Ω factor is ignored since the PFC free energy is expressed as per volume rather than per atom.

The PFC density parameter n is related to atomic density ρ of the material by $n = (\rho - \bar{\rho})/\bar{\rho}$ where $\bar{\rho}$ is a reference density. The same relation holds for the long-range-averaged value $n_{mf} = (\rho_{mf} - \bar{\rho})/\bar{\rho}$. The atomic concentration can then be related to the long-range-averaged atomic density ρ_{mf} by $c = \Omega\rho_{mf}$; then the long-range-averaged PFC density parameter n_{mf} can be linked to the atomic concentration by

$$c = \Omega(n_{mf} + 1)\bar{\rho}. \tag{13}$$

Since the length scale corresponding to the lattice spacing has been averaged out in the calculation of f_a [Eq. (10)], one may expect that $\frac{\partial f_a}{\partial n_{mf}}$ can somehow approximate the long-range behavior of the functional derivative $\delta F/\delta n$ in the PFC equation of motion [Eq. (2)]. Using this ansatz (which will be examined later using numerics), one can map the long-range behavior of $\nabla\frac{\delta F}{\delta n}$ in the PFC equation to the pressure gradient ∇P in the continuum description since

$$\nabla\frac{\delta F}{\delta n} \sim \nabla\frac{\partial f_a}{\partial n_{mf}} \sim \nabla P/(k_BT\bar{\rho}), \tag{14}$$

where Eqs. (11) and (12) are used.

With the concentration expression in Eq. (13) and the pressure expression in Eq. (14), the pressure-induced atomic current $J_p = -Mc\Omega\nabla P$ can be incorporated in the PFC equation using

$$J_P^{PFC} = -Mk_BT\bar{\rho}^2\Omega^2(1+n_{mf})\nabla\frac{\delta F}{\delta n}. \tag{15}$$

The EM-induced atomic current $J_{\rm em} = McZ^*eE$ can be expressed in a similar way in the PFC model

$$J_{\rm EM}^{PFC} = M\bar{\rho}\Omega(1+n_{mf})Z^*e\vec{E} = M\bar{\rho}\Omega(1+n_{mf})Z^*e\nabla V, \tag{16}$$

where V is electric potential. The PFC equation of motion that incorporates both the EM-driven and the pressure-driven atomic fluxes is then

$$\frac{\partial n}{\partial t} = \nabla\cdot\Gamma\left[\bar{\rho}\Omega(1+n_{mf})\nabla\frac{\delta F}{\delta n} - (1+n_{mf})\frac{Z^*e\vec{E}}{k_BT}\right], \tag{17}$$

where $\Gamma = M\bar{\rho}\Omega k_BT$. It is noted that Eq. (17) is different from the variational formulation in the original PFC EM model [i.e., Eq. (2)], whose coupling to $\vec{E}$ arises only through the free energy in the pressure term. It is noteworthy, however, that it goes back to the variational form in the limit where n_{mf} can be treated as a constant and $\bar{\rho}\Omega = 1$.

V. NUMERICAL ALGORITHM

The equation of motion for the PFC EM model is

$$\frac{\partial n}{\partial t} = \nabla\cdot\Gamma\left[\bar{\rho}\Omega(n_{mf}+1)\nabla\frac{\delta F}{\delta n} - (n_{mf}+1)\frac{Z^*e\vec{E}}{k_BT}\right], \tag{18}$$

where $\Gamma = M\bar{\rho}\Omega k_BT$ and the electric field satisfies the current continuity equation

$$\nabla\cdot(\sigma\vec{E}) = 0, \tag{19}$$

with σ being the conductivity. Both equations are solved in 2D in the Fourier space.

Equation (18) can be rewritten as

$$\frac{\partial n}{\partial t} = \Gamma\bar{\rho}\Omega\nabla^2\frac{\delta F}{\delta n} + \nabla\cdot\left[\Gamma\bar{\rho}\Omega n_{mf}\nabla\frac{\delta F}{\delta n} - (n_{mf}+1)\frac{Z^*e\vec{E}}{k_BT}\right]. \tag{20}$$

By treating the second term on the right as a nonlinear term, Eq. (20) can be solved efficiently with the semi-implicit algorithm discussed in Ref. [27]. The microstructure-dependent conductivity in Eq. (19) can be written as $\sigma(\vec{r}) = \sigma_0 - \sigma_1(\vec{r})$ where σ_0 is a constant and $\sigma_1(\vec{r})$ is the conductivity deviation due to the microstructure at point $\vec{r}$. Given an initial microstructure-independent electric field $\vec{E}^0$, the microstructure-dependent electric field can be obtained by iteratively solving

$$\nabla\cdot(\sigma_0\vec{E}^{(n+1)}) = \nabla\cdot[\sigma_1(\vec{r})\vec{E}^{(n)}], \tag{21}$$

where $\vec{E}^{(n)}$ is electric field from the nth iteration. Equation (21) can be rewritten using the electric potential V as

$$\sigma_0\left(\frac{\partial^2V^{(n+1)}}{\partial x^2} + \frac{\partial^2V^{(n+1)}}{\partial y^2}\right) = \frac{\partial A_x^{(n)}}{\partial x} + \frac{\partial A_y^{(n)}}{\partial y}, \tag{22}$$

where $A_x^{(n)} = \sigma_1(\vec{r})E_x^{(n)}$ and $A_y^{(n)} = \sigma_1(\vec{r})E_y^{(n)}$ with $E_x^{(n)}$ and $E_y^{(n)}$ being the x and y components of the electric field from the nth iteration. By replacing V, A_x, and A_y with their Fourier transform $g(\vec{r}) = \int\tilde{g}(\vec{k})e^{-i\vec{k}\cdot\vec{r}}d\vec{k}$, where g can be V, A_x, or A_y, and $\vec{k}$ is the wave number. Equation (22) in the Fourier space becomes

$$\tilde{V}^{(n+1)}(\vec{k}) = \frac{ik_x\tilde{A_x}^{(n)} + ik_y\tilde{A_y}^{(n)}}{\sigma_0\left(k_x^2+k_y^2\right)}, \tag{23}$$

where k_x and k_y are the x and the y components of $\vec{k}$. The real-space potential field $V^{(n+1)}$ is obtained through the inverse Fourier transform of the $\tilde{V}^{(n+1)}$ from Eq. (23). The $V^{(n+1)}$ can then be used to calculate the electric field and reevaluate A_x and A_y for the next iteration. The microstructure-dependent electric field E satisfying Eq. (19) is then obtained by iterating Eq. (23) until $|E^{n+1} - E^n|$ is smaller than a threshold.

In all the 2D numerics, the spacings of the spatial mesh are set to $dx/a = 3/32$ and $dy/a = \sqrt{3}/16$. Those values are chosen such that the simulation box contains an integer number of lattice spacing a along both the x and y directions. Also $\bar{\rho}\Omega = 1$ and $\Gamma = 10$ are used in all simulations unless explicitly specified.

VI. RESULTS AND DISCUSSION

Numerical results demonstrating continuum and atomistic features of the PFC EM model are discussed in this section.

The important ansatz from the continuum EM theory part, where the long-range behavior of the PFC equation of motion is connected to the established continuum EM theories, is examined numerically here. Numerical results for the pressure evolution from the PFC EM model in Eq. (17) are shown in Fig. 1. One can see from Fig. 1 that the pressure profile gradually develops from the initial transient state toward the flux-balanced state given by $dP/dx = Z^*eE/\Omega$. The theoretical pressure profile is simply calculated by drawing a line with slope Z^*eE/Ω with zero pressure at the center of the simulation domain. This proves the ansatz that the PFC model includes the continuum flux-balancing condition as its long-range behavior, and it is a strong validation for the PFC approach in Eq. (17) since the Blech effect in continuum EM theory is quantitatively reproduced.

The PFC EM model reproduces the well-established Blech effect on continuum scales; as shown in Fig. 1 and Ref. [21], its ability in capturing atomic-scale structural evolution at diffusional timescales makes it a potentially useful method in understanding the current-driven microstructure evolution at nanoscales. Motion of surface steps driven by EM is an important process that has long been associated with EM-induced failure. Using the PFC EM model, EM-driven motion of surface steps is examined. Figure 2 shows a time sequence of the EM-driven step motion. As the electron wind is blowing from the right to the left, lattice atoms tend to move in the same direction as the electron wind due to the EM force from electron scattering. For a step edge shown in Fig. 2, this EM-induced one-direction motion of atoms to the left results in the motion of the step edge toward the right as atoms on the edge were transported away from the step by the EM process. As suggested in previous experiments and quantum

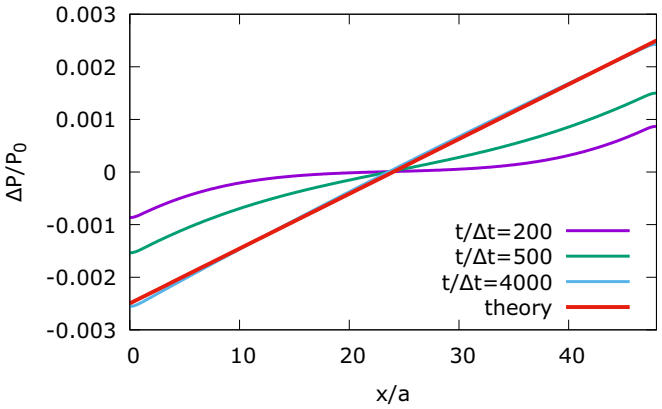

FIG. 1. Pressure development in the conducting material under a given electric field $eEa/(k_BT) = 0.002$. The three solid lines are the pressure profiles at different times. $\Delta P = P - P_0$. The dashed line is the theoretical pressure profile given by $dP/dx = Z^*eE/\Omega$. Simulation pressures are averaged over the simulation domain height $h/a = 12$. Effective EM charge $Z^* = -1.0$. PFC parameters are $r = 0.13$, average density $\bar{n} = 0.1867$ which is the equilibrium density at the given r, and other parameters are $(dt, dx, dy, B_x, \alpha, b, c, \lambda) = (1.0, \sqrt{3}\pi/8, \pi/4, 0.7, 50, -19, 50, 0.05)$. P_0 is the zero-current stress. The stress in this figure is calculated numerically from the equilibrated PFC density profile instead of the one-mode approximation in Eq. (9). Only half of the simulation system length is shown in the figure; the other half is a mirror image of the first half with respect to the $x = 0$ plane. This setting is to satisfy the periodic boundary condition for the electric potential field. Noise is set to zero in the simulation.

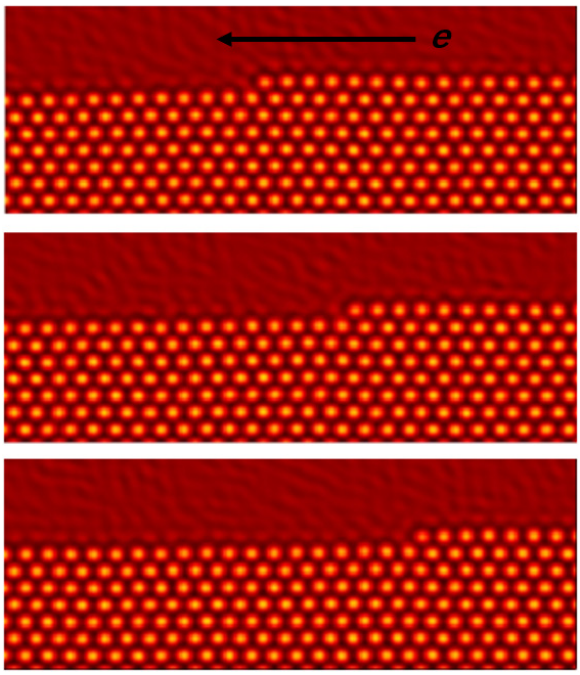

FIG. 2. Plots of PFC atomic density field $n(\mathbf{r})$ showing a time sequence in the evolution of step motion (from top to bottom) driven by EM. Direction of electron current is from the right to the left as shown by the arrow. The periodic regions of the PFC density parameter in the figures (lower half) represent the solid phase, while the uniform regions in the figures (upper half) is the coexisting vapor phase. A surface step (at the solid-vapor interface) is shown to move in the opposite direction of electron current. PFC parameters are the same as in Fig. 1 except for $r = 0.11$ and $\bar{n} = 0.19$. Only the region near the surface step was shown in the figure. For the whole simulation system, the same mirror image setup as in Fig. 1 was used. The system was carefully initiated with a partially covered layer of atoms at the solid-vapor interface.

mechanical calculations [9], the effective EM charge on a material's surface can be significantly enhanced compared to its bulk value. Since the surface step motion can be well captured in the current PFC model, one can easily incorporate this enhanced surface EM effect.

While the result shown in Fig. 2 is not based on a realistic metal system, quantitative EM results can be obtained by using the effective EM charge and tuning the PFC model to match the elastic properties of the material as demonstrated in Fig. 1. The matching of the PFC model to realistic materials has been discussed in other literature [39,40]. Since the current PFC EM model is built on the effective-charge-based EM description which is mainly used for metal systems, it should not be applied to semiconductors without further validations.

The results in this work were all obtained using 2D numerics; the authors would expect very similar results from full 3D calculations although the computational cost for such calculations will be rather expensive.

VII. SUMMARY

This work connects a previously proposed PFC electromigration model to quantum mechanical EM theories and macroscopic diffusion flux based continuum EM theories. The connection to the quantum mechanical theories is explained based on electronic and classical density functional theories, while the connection to diffusion-based continuum theories is achieved by coarse-graining the free energy functional in the PFC model. A quantitative agreement between the PFC EM model and the well-established Blech effect in continuum EM theories is demonstrated. The capability of incorporating enhanced EM forces on atomic-scale defects while tracking the microstructure evolution over long timescales makes the PFC EM model a potentially useful tool in understanding current-driven microstructure changes in conducting materials.

ACKNOWLEDGMENTS

The authors thank the National Science and Engineering Research Council of Canada and the Canada Research Chairs Programs for funding, and Compute Canada for HPC resources. N.W. also acknowledges the startup support of Guangdong Technion–Israel Institute of Technology and the computer time from GTIIT High Performance Computing Center.

[1] K. N. Tu, J. Appl. Phys. **94**, 5451 (2003).
[2] R. L. de Orio, H. Ceric, and S. Selberherr, Microelectronics Reliability **50**, 775 (2010).
[3] R. M. Feenstra and B. G. Briner, Superlattices Microstruct. **23**, 699 (1998).
[4] C. Tao, W. G. Cullen, and E. D. Williams, Science **328**, 736 (2010).
[5] R. Yongsunthon, C. Tao, P. Rous, and E. D. Williams, in *Nanophenomena at Surfaces*, edited by M. Michailov, Springer Series in Surface Sciences, Vol. 47 (Springer, Berlin, 2011), Chap. 5.
[6] R. Hoffmann-Vogel, Appl. Phys. Rev. **4**, 031302 (2017).
[7] P. Kumar and R. S. Sorbello, Thin Solid Films **25**, 25 (1975).
[8] R. S. Sorbello, Phys. Rev. B **23**, 5119 (1981).
[9] K. H. Bevan, H. Guo, E. D. Williams, and Z. Zhang, Phys. Rev. B **81**, 235416 (2010).
[10] I. A. Blech, J. Appl. Phys. **47**, 1203 (1976).
[11] J. R. Lloyd, J. Appl. Phys. **69**, 7601 (1991).
[12] E. Arzt, O. Kraft, W. D. Nix, and J. E. Sanchez, J. Appl. Phys. **76**, 1563 (1994).
[13] D. Maroudas, Surf. Sci. Rep. **66**, 299 (2011).
[14] N. Wang and N. Provatas, Phys. Rev. Appl. **7**, 024032 (2017).
[15] S. S. Lyer, MRS Bulletin **40**, 225 (2015).
[16] J. M. Campbell and R. G. Knobel, Appl. Phys. Lett. **102**, 023105 (2013).
[17] J. Taylor, H. Guo, and J. Wang, Phys. Rev. B **63**, 245407 (2001).
[18] S. Heinze, N.-P. Wang, and J. Tersoff, Phys. Rev. Lett. **95**, 186802 (2005).
[19] H. Löwen, J. Phys.: Condens. Matter **14**, 11897 (2002).
[20] K. R. Elder, N. Provatas, J. Berry, P. Stefanovic, and M. Grant, Phys. Rev. B **75**, 064107 (2007).
[21] N. Wang, K. H. Bevan, and N. Provatas, Phys. Rev. Lett. **117**, 155901 (2016).
[22] R. S. Sorbello, J. Phys. Chem. Solids **34**, 937 (1973).
[23] M. te Vrugt, H. Löwen, and R. Wittkowski, Adv. Phys. **69**, 121 (2020).
[24] M. Haataja, L. Gránásy, and H. Löwen, J. Phys.: Condens. Matter **22**, 360301 (2010).
[25] K. R. Elder and M. Grant, Phys. Rev. E **70**, 051605 (2004).
[26] Z.-F. Huang and K. R. Elder, Phys. Rev. B **81**, 165421 (2010).
[27] G. Kocher and N. Provatas, Phys. Rev. Lett. **114**, 155501 (2015).
[28] V. Fallah, A. Korinek, N. Ofori-Opoku, N. Provatas, and S. Esmaeili, Acta Mater. **61**, 6372 (2013).
[29] J. Berry, N. Provatas, J. Rottler, and C. W. Sinclair, Phys. Rev. B, **89**, 214117 (2014).
[30] G. Kocher and N. Provatas, Phys. Rev. Materials **3**, 053804 (2019).
[31] W. Kohn and L. J. Sham, Phys. Rev. **140**, A1133 (1965).
[32] V. Heine and D. Weaire, Solid State Phys. **24**, 249 (1970).
[33] J.-P. Hansen and I. R. McDonald, *Theory of Simple Liquids* (Elsevier, 1990).
[34] T. V. Ramakrishnan and M. Yussouff, Phys. Rev. B **19**, 2775 (1979).
[35] K. H. Bevan, W. Zhu, G. M. Stocks, H. Guo, and Z. Zhang, Phys. Rev. B **85**, 235421 (2012).
[36] M. Di Ventra, Y. C. Chen, and T. N. Todorov, Phys. Rev. Lett. **92**, 176803 (2004).
[37] J. P. Dekker, A. Lodder, and J. van Ek, Phys. Rev. B **56**, 12167 (1997).
[38] S. van Teeffelen, C. V. Achim, and H. Löwen, Phys. Rev. E **87**, 022306 (2013).
[39] K.-A. Wu and A. Karma, Phys. Rev. B **76**, 184107 (2007).
[40] E. Asadi and M. A. Zaeem, Comput. Mater. Sci. **105**, 101 (2015).